Advanced Radar Geosynchronous Observation System - ARGOS

Andrea Monti Guarnieri, *member, IEEE*, Antoni Broquetas, Andrea Recchia, Fabio Rocca, Josep Ruiz Rodon

***Abstract*— ARGOS is proposed to be a Multiple Inputs Multiple Outputs (MIMO) Synthetic Aperture RADAR (SAR) system hosted on a swarm of mini satellites in quasi-geostationary orbits. The system is made of N iso-frequency sensors, each of them transmitting and receiving the signals. The system would combine the continuous imaging capabilities of a geostationary SAR, gaining a factor N^2 in Signal-to-Noise ratio. The real aperture would be achievable in ~40 minutes, enabling applications so far unseen like monitoring fast deformations, landslides, and other applications for emergency and security. Still, the SNR of the long acquisition time would be conserved. The optimal design of the swarm is addressed, in order to trade resolution, coverage and revisit time.**

***Index Terms*— MIMO radar, Synthetic aperture radar, Spaceborne radar, Radar interferometry, Earth Observing System**

I. INTRODUCTION

GEOSYNCHRONOUS SAR's exploits orbit eccentricity and inclination to get a suitable synthetic aperture, whereas the strong path loss attenuation is compensated by means of both medium-to-long term integration time, large transmitted power and large antenna reflectors. Two concepts have so far been proposed: the geosynchronous and the quasi-geostationary SAR. The *geosynchronous* SAR, shown in Fig.1 (top), first proposed in [1], achieves a continental coverage and one-day revisit by exploiting significant orbit inclination and eccentricity. Spread losses are compensated by huge antenna and high power, that would require 2020 technologies [2]. It is getting growing interest in recent literature [3][4][5].

The *geostationary* SAR with regional coverage is represented in Fig.1 (bottom) in the original bistatic configuration **Error! Reference source not found.**. The system compensates spread losses by long integration times (hours), and therefore exploits moderate power and medium size antennas. It is then suited to be embarked as a monostatic payload of opportunity on a COMmunication SATellite (COMSAT) [7]. In that case, the maximum allowed orbit jitter of ±0.1° would leave a synthetic aperture of 150 km, that in turn allows generating SAR images in a continuous trade-off between observation and resolution that scales from ~100 m in 20 minutes to 5 meters in 8 hours in X band. Such quasi-continuous imaging capability is an unique feature of geostationary SAR, that enables a wide variety of applications, some unprecedented, like the estimation of water-vapor maps at fine resolution on land for Numerical Weather Predictions, detecting precursors for landslides or eruption hazards monitoring (see [8] for an overview).

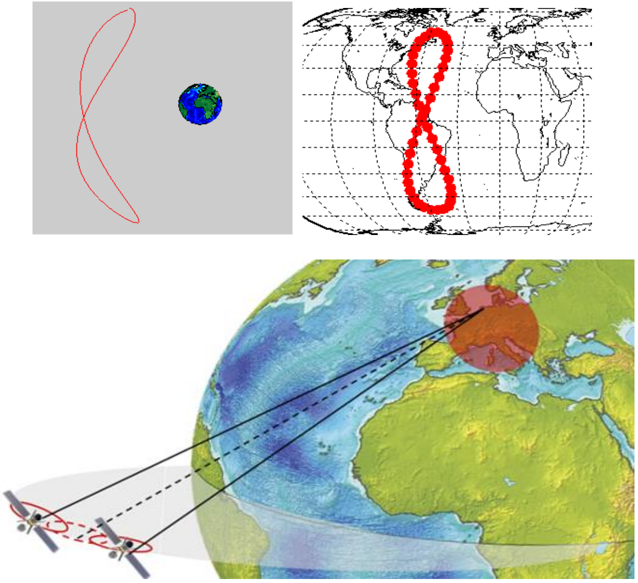

Fig.1 Top pictures: orbit (in scale) and nadir track of a typical geosynchronous SAR with continental coverage, characterized by a significant inclination and eccentricity. Bottom picture: representation of a bistatic quasi-geostationary SARs with regional coverage, whose orbit has near zero inclination and small eccentricity. The dotted lines refer to its monostatic equivalent

Nonetheless, geostationary SAR image quality is impaired by both the Atmospheric Phase Screen (APS) [3][9][10][11], and by backscatter decorrelation in the 1-day revisit. The mitigation of decorrelation demands for long wavelengths, and in fact typically L band is proposed for GEO-SAR. However, this choice limits the achievable azimuth resolution to say 1.3 km, single look, after 20 minutes of synthetic aperture, down to 40 m in 7-8 hours. This reduces the observation capabilities and the applications to wide scale monitoring.

In this paper, we propose a different concept, named ARGOS from the mythological 100-eyed giant, that is an enhancement of the geostationary SAR. ARGOS bases on a swarm of N iso-frequency mini-satellites in closed flight formation [12], a MIMO SAR [13][14] with $N_{TOT}=N\times(N+1)/2$ center of phases that are displaced along longitudes to sample the synthetic aperture. In the following, we assume N=6 as this is the number of mini-satellites of less than 300 kg payload, that could be launched simultaneously by an Ariane 5 class launcher. The formation, by tessellating and parallelizing the scan of the Doppler frequencies axis, allows to generate a new image in about 40 minutes, while maintaining the SNR correspondent to the long acquisition time with a single satellite. Being free from clutter and atmospheric artifacts, the system could benefit of the large bandwidths and the small antennas typical of X band. Furthermore, the freedom degrees in tuning the orbit parameters give space to different configurations of the swarm, where resolution can be traded in flight for coverage, or revisit time.

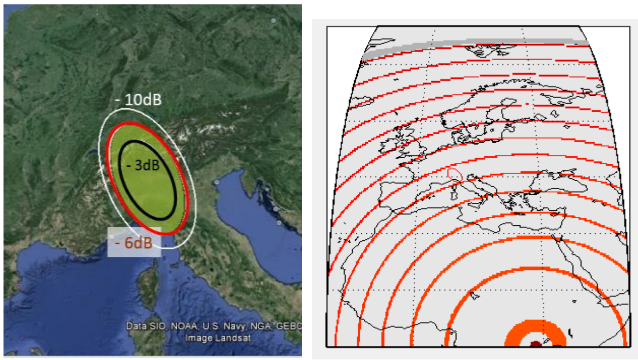

Fig. 2 X-band monostatic geostationary SAR. Left: antenna footprint, 250×430 km at -6 dB. Right: dartboard diagram [7] for PRF=340 Hz, duty cycle 10%.

II. MONOSTATIC GEOSTATIONARY SAR: DESIGN AND PERFORMANCES

Each single monostatic satellite's orbit around a fixed reference on Earth can be described in polar coordinates [15]:

$$r(t) = R_{geo}\left(1 - 2e_n \cos\left(\Omega_E\left(t - t_n\right)\right)\right) \qquad (1)$$
$$\psi(t) = \psi_n + 2e_n \sin\left(\Omega_E\left(t - t_n\right)\right)$$

R_{geo}=42164.2 km is the average geosynchronous orbit radius, Ω_E=2π/86400 the earth angular speed, r(t) is the instantaneous orbit radius, and ψ(t) the instantaneous longitude. The orbits in (1) describe small ellipses, like those shown in Fig. 1, centered at latitude ψ_n and with eccentricity e_n. The parameter t_n is the reference time chosen at the satellites cross over the perigee. In (1) zero orbit inclination is assumed to avoid baseline decorrelation [7], as this is not relevant for the synthetic aperture, though a slight inclination could be introduced for a safe constellation keeping [17]. We have also ignored a longitude drift [12], indeed quite small. The small baselines considered limit cross track resolution and then tomographical applications, that need a different L band constellation [16].
The orbit of each satellite in the swarm is then fully described by the tern of parameters {ψ_n, e_n, t_n}. The eccentricity plays a fundamental role, as it fixes the along track angle span, $\Delta\psi_n$=4e_n, therefore the synthetic aperture, L_{sn} and the resolution, ρ_{azn}, of each monostatic system:

$$L_{sn} = 4R_{geo}e_n \qquad \rho_{azn} = \frac{\lambda}{2L_{Sn}}R = \frac{\lambda R}{8R_{geo}e_n} \qquad (2)$$

λ being the wavelength and R the satellite-target distance ~38000 km at 45° latitude. Notice that the variation of the orbit radius, r(t) in (1), is irrelevant as for the synthetic aperture. The azimuth resolution in (2) can be made pretty good, ~5 m, by assuming X band and the maximum eccentricity allowed for a COMSAT, e ~8·10^{-4}. Achieving that resolution would not be simple, since the design of the monostatic system is constrained by the severe path loss, then by SNR [6][7]:

$$SNR = \frac{P_t G A \eta_T}{\left(4\pi R^2\right)^2} \frac{\sigma^0 \rho_{az} \rho_{rg}}{\sin\theta} \frac{T_S}{N_0} = \frac{P_t G A \eta_T}{\left(4\pi\right)^2 R^3} \frac{\sigma^0 \rho_{rg} \lambda}{2v_s \sin\theta} \frac{1}{N_0} \qquad (3)$$

P_t being the mean transmitted power, G and A the antenna gain and area, η the total losses, σ^0 the backscatter coefficient, θ the incidence angle, ρ_{az}, ρ_{rg} the azimuth and range resolution, N_0 the noise power spectrum, T_s the synthetic aperture time and v_s the mean velocity in the useful aperture interval. The rightmost expression, derived by exploiting (2), shows that SNR, and then NESZ, are independent upon the observation time, for the distributed target case, since the synthetic aperture time and the azimuth resolution are inversely proportional.
Performances are summarized in Tab. I for the X band system located at 28° longitude shown in Fig. 2, and referred to an image resolution of 20×20 m, 4 looks. The SNR is 4 dB at the swath edges for an average transmitted power P_t=150 W.

TABLE I
GEOSTATIONARY MONOSTATIC SAR DESIGN, X BAND

Parameter	**Unit**	**Value**		
		Near Range	Mid Range	Far range
Polarization			HH	
Ground Range resolution	m	21	20	19
Azimuth resolution:				
coarse (40 min)	m		54	
fine (12 hour)	m		5	
Mean power	W		150	
Antenna Directivity	dB	49.5	52.5	49.5
Antenna Eq. Area	dBsm	8.38	11.4	8.38
EIRP	dB_W		19.0	
Path losses	dB	-162.6	-162.6	-162.7
Total losses	dB		-4.0	
Target backscatter	dBsm	-11	-11.6	-11.8
Noise spectrum density	dB_W		-202	
NESZ	dB	-16.1	-21.2	-16
SNR	dB	4.8	9.6	4.2

The quick-look azimuth resolution, say in 40 minutes aperture, is pretty coarse even in X band, 50 m, while the swath width is actually constrained by the limited power. Furthermore, data quality is impaired by the decorrelation that occurs in the one-day interferometric revisit and from tropospheric turbulence.

Examples of correlation matrixes acquired in different scenes of grass and short vegetation, and different seasons, using a Ku-band ground based SAR [9] are shown in Fig. 3. Coherence is lost from day to day, and during the day within hours. This prevents any interferometric applications unless relying on Persistent Scatterers, [16], that give limited results at such coarse resolution.
On the top of this, the Atmospheric Phase Screen adds further decorrelation, in the long integration time (minutes), that can be so strong to demand for L band as a safe choice [3][4][10]. The APS decorrelation shown in Fig. 4 has been computed according to [11] and by assuming a space-time APS variogram (that is the standard deviation of the differential delay measured in two targets ad distance r meters, after t seconds):

$$\sigma^2_{aps}(t,x) = 2\sigma_{APS}{}^2\left(\sqrt{\left(\frac{t}{t_0}\right)^2 + \left(\frac{r}{r_0}\right)^2}\right) \qquad (4)$$

where the APS time and space constants were assumed t_0 =10 hours and r_0=20 km. It appears from Fig. 4 that practical values of σ^2_{APS} in the range 400-800 mm^2 lead to significant "clutter" for images taken in X band during an aperture of say one hour, whereby an aperture of 20 minutes would quite get a moderate clutter at all frequencies up to Ku-band.

III. GEOSTATIONARY SWARMS

The combination of two satellites, each transmitting and receiving, results in three phase centers, the third one spanning the equivalent elliptical orbit shown in Fig.1. In the case of N=6 geosynchronous mini-satellites so far discussed, an ideal uniform distributions of the N_{TOT}=21 phase centres, as many as the combination with repetition, would get a full real aperture in 12 hours / 21 ~ 35 minutes. This is the overall fine resolution image time, whereas the interferogram revisit would be in the average half of that, 20 minutes. In such time, the impact of scene decorrelation [6], also known in lunar SAR papers [18][19], and atmospheric phase screen will be de-criticized, as shown in Fig. 3 and Fig. 4.

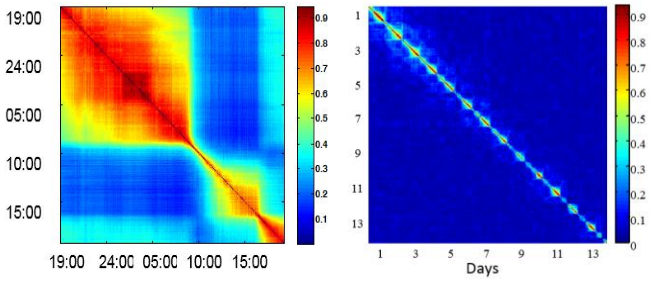

Fig. 3 Examples of Ku-band correlation matrixes over grass fields, from different ground based SAR acquisitions. Left: one day, area of Berne (CH), spring, and, right, 12 days, area of Beauregard (Italy), summer.

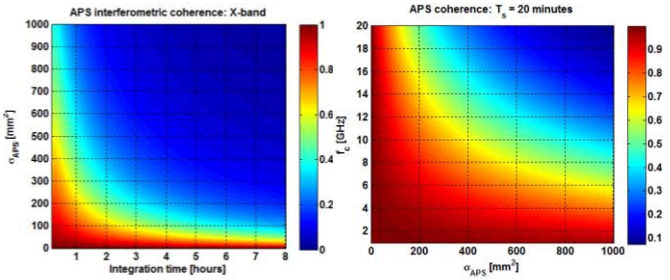

Fig. 4 Decorrelation due to the uncompensated Atmospheric Phase Screen computed according to [15]. Left: X band case, and function of σ_{APS} and integration time. Right: 20 minutes integration time and function of σ_{APS} and frequency.

A. Link budget

In order to evaluate the **link budget,** the intuitive way is to say that we have six transmitters and six receivers so the total power is six times, and the same goes for the receiving area, so in total we achieve a gain of 36 with respect to the monostatic case.

Another way to arrive to the same result, maybe more acceptable, is the following. Let us consider any monostatic or bistatic couple. In the real aperture time, say 40 minutes, each couple operates on an azimuth resolution that is approximately 1/21 the total. Combining the different monostatic/bistatic systems, we achieve full azimuth resolution indeed, but the SNR is the one calculated with the low resolution. This gives us a factor N_{TOT}=21. Then, we have to consider the double takes, namely when satellite A is transmitting and satellite B is receiving and vice versa, while they are illuminating the very same wave number. Here we have to sum the two energies: in total we have that the factor 21 has to be augmented by the probability of each wave number being covered twice, and therefore has to be multiplied times the factor f={1+15/21}. In conclusion 21·f=36 or N×(N+1)/2+N×(N-1)/2=N^2.

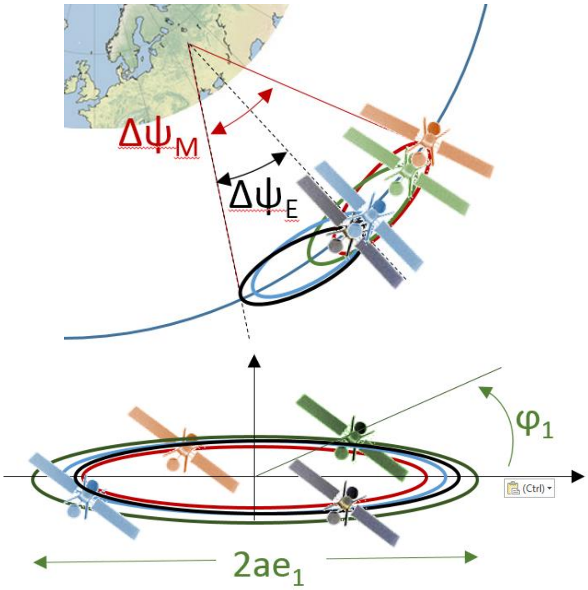

Fig. 5 Swarm configurations. Above: ISO-elliptical, below: concentric

Now, if we integrate the return signal in this time interval, we get the link budget as from (3):

$$SNR = 6 \times 6 \frac{P_t G A \eta_T}{(4\pi)^2 R^3} \frac{\sigma^0 \rho_{rg} \lambda}{2 v_s \sin\theta} \frac{1}{N_0} \tag{5}$$

In this case, the observation time therefore will be taken to be about 2400 seconds, as the real antenna is not fully sampled before that time. The gain by a factor 36 can be traded to achieve fine resolution while keeping constant SNR in (3): the 54×20 m resolution cell achieved after 40 minutes in the monostatic configuration of Tab. I would correspond to $54 \times 20/36$ ~ 5.4×5.4 meters in the MIMO. Then after 40 minutes, the antennas either could be steered towards a different target or could stay, improving stable targets imaging.

IV. ARGOS CONFIGURATIONS

The eccentricities, the ascending node times and the centre longitudes are free parameters that can be tuned to configure and re-configure the constellation according to applications. In this section, we propose two different configurations, represented in Fig. 5. In the **ISO-elliptical** configuration, all the satellites move synchronously with respect to fixed Earth, that is with the same eccentricity vectors, $\mathbf{E}_n$:

$$\mathbf{E}_n = e_0 \exp\left(j \Omega_E t_0\right) \tag{6}$$

The orbits in (1) just differs by the central longitudes, ψ_n, to be optimized for all the satellites but the two extreme. In the **concentric** configuration, all the satellites share the same longitude, but with different eccentricity vectors to be optimized.

A. *ISO elliptical Swarm*

In the ISO-elliptical swarm, shown in the upper graph in Fig. 5 the orbits share the same eccentricity vectors, therefore the freedom degrees are the N-2 central longitudes ψ_n (n=2..N-1); the absolute eccentricity e_0; the overall span of the constellation, $\Delta\psi_M$ shown in the figure.

The idea in this configuration is to keep fixed the angular shift of the satellites with time. The result after optimization on the four central longitudes is the one shown in Fig. 6: the instantaneous angles of all the 36 phase centres, proportional to the Doppler, are in the upper left plot. At each time, the total angular aperture spanned, $\Delta\psi_M$, gives an image resolution (2):

$$\rho_{az} = \frac{\lambda}{2R_{geo}\Delta\psi_M}R \tag{7}$$

The mean angle sweeps as a sinus with time, leading in 24 hours to a total "extra fine resolution":

$$\rho_{az\_24} = \frac{\lambda}{2R_{geo}\left(\Delta\psi_M + \Delta\psi_E\right)}R \tag{8}$$

When $\Delta\psi_M$ gets larger than $\Delta\psi_E$, resolution gets coarse, but image time and revisit reduces. In the example shown in the figure, $\Delta\psi_E$ has been equated to $\Delta\psi_M$.

The optimization has been run with the goal of minimizing the difference between the maximum and minimum distances of phase centres (that stay fixed with time):

$$g = \max\left(\psi_n - \psi_m\right) - \min\left(\psi_n - \psi_m\right) \tag{9}$$

and adding a penalty to avoid coincident phase centres. This difference is in the bottom-right plot in the figure.

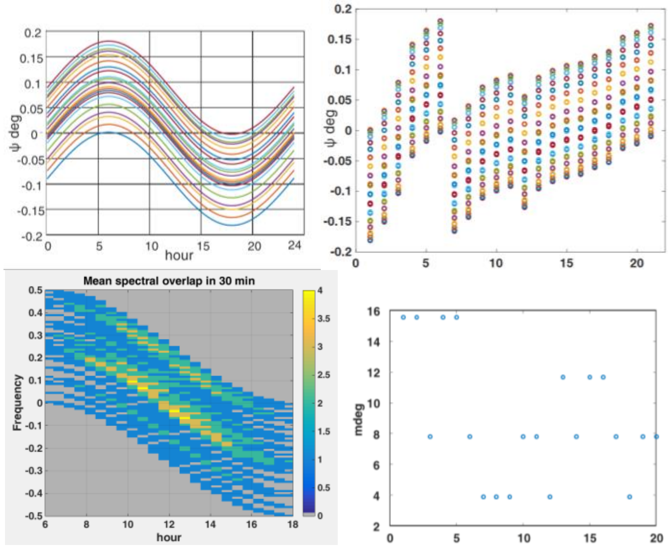

Fig. 6 Iso elliptical optimized swarm. Up-left: angles spanned by each phase centre as function of time. Up-right: superposition of all the angles, the first 6 columns corresponding to the satellites orbits, the others to the equivalent monostatic. Bottom: spectral overlaps in 30' and angles differences.

In order to assess the effective image time, histograms of angles spanned in 30 minutes intervals have been computed all along half an orbit, and shown in the lower-left panel in Fig. 6. The spectral coverage is better than 80% for 75% of the time. It would be interesting to achieve the best coverage at dawn and early morning, where best performances are expected due to both scene coherence (see Fig. 3), and calm APS [9].

1) *Separation in the Doppler domain*

At a first glance one would think that the duty cycle is to be made N times smaller, as all the satellites have to be enabled to transmit, in turn. However, this drawback could be avoided by letting all SAR transmitting simultaneously and then separating the different contributions in the Doppler domain. We could do it if the Doppler bandwidth B_R, spanned during the real aperture time, T_R, is much smaller than the instantaneous Doppler shift between to closest equivalent monostatic phase centers B_m:

$$B_D = \frac{2v_s}{\lambda}\frac{\lambda}{v_s T_R} << B_m = \frac{2v_s}{\lambda}\frac{\Delta\psi_M}{21} \tag{10}$$

Then, by combining with (7)

$$\frac{1}{T_R} << \frac{v_s}{\lambda}\frac{\lambda R}{21\cdot 2\rho_{az}R_{geo}} \approx \frac{v_s}{42\cdot\rho_{az}} \Rightarrow T_R >> \frac{42}{v_s}\rho_{az}$$

That is satisfied with good margin if we consider a resolution in the order of few meters and a real aperture time of tens of minutes, and a typical value v_s~5 m/s.

B. *Concentric swarm*

The non-uniform spectral coverage with time can be avoided by the dual configuration, the concentric swarm, achieved by assuming all sensor's orbit concentric and tuning the eccentricity vectors, as shown in Fig. 5, in a carthwheel like configuration [12]. In this case, the optimization has been carried out by maximizing the spectral coverage, say by minimizing the number of spectral holes shown in the bottom left picture in Fig. 7.

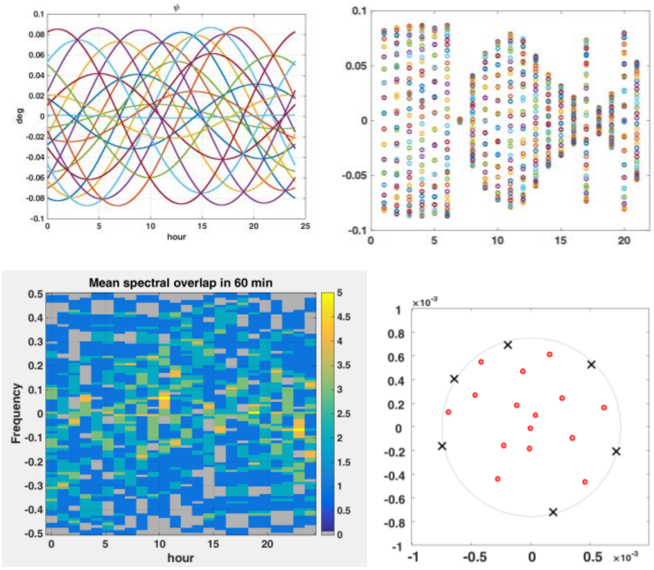

Fig. 7 Concentric optimized swarm. The spanned angles with time, Up-left, and angles, up-right, are the same as for Fig. 6. The bottom-left histograms of spectral overlaps are here measured over 60' intervals. Bottom-right: eccentricity vectors of the satellites ('X') and the monostatic equivalents ('o').

Notice that the coverage is random, but the result is uniform all over orbit time. The eccentricity of the satellites orbits, marked by 'X' in the lower right plot, are almost constant in amplitudes, whereas their phases are unevenly spaced, as to avoid concentrations close to the origin of the equivalent monostatic orbit's eccentricity. This means that we could just optimize the N-1 arguments of eccentricities, getting a dual design respect to the ISO-elliptical configuration. The spectral coverage, shown in Fig. 8 on the right, is better than 80%. Spectral holes can be handled by interpolating the 12-hours observations.

CONCLUSIONS

We have introduced a new GEO-SAR concept that is based on an iso-frequency swarm of mini-satellites. A comparison between this and other space-borne SARs is given in Tab. II. The system gets several advantages with respect to a single geosynchronous SAR.

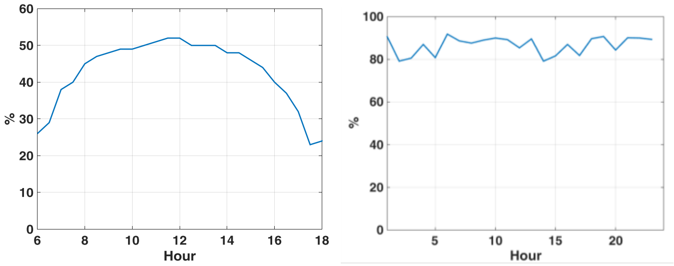

Fig. 8 Percentage of spectral coverage in 30' for ISO.elliptical configuration (left) and 60' for concentric configuration (right).

A fine resolution image is achieved in a much shorter time, say 30' in place of 8h, and furthermore the resolution is decoupled from the wavelength, leaving space for application – based optimizations. Moreover, having completed an image in 30', we are able to reconfigure the sensor's operative modes, i.e. achieving a different tradeoff between coverage and resolution.

A second set of advantages of the swarm stays in the fact that the global receiving antenna is 6 times larger than in the monostatic case and the transmitting power 6 times larger for the multiplicity of the transmitters. So, the overall size approaches that of the high inclination case (the Tomiyasu's figure of 8, in Fig. 1). The N^2 gain in SNR can then be exploited to shorten the image time and shrink the resolution cell.

TABLE II

COMPARISON BETWEEN GEO AND LEO SAR CONCEPTS

	GEO SYNCHRONOUS	**GEO STATIONARY**		**LEO**
		MONOSTATIC	SWARM	
Coverage	Continental	Regional (limited by SNR)	Regional	World
Orbit	Significant inclination	Δlong<±0.1° Small eccentricity		
Image time	Minute(s)	20 min: quick look 7 hr: full res.	**40 minutes: full resolution**	< 1 sec
APS	Almost Frozen	Sensed - To be compensated	**Sensed and compensated**	Frozen
Line Of Sight	East-West	North-South	North-South	East-West
Revisit time	Once a day	Twice a day	**40 minutes**	Days
System	Dedicated sensor, 2020+ technologies	Payload on a GEO COMSAT	Swarm of mini satellites	Dedicated satellite

A final advantage is the graceful degradation in the case of single failures. The receivers of possible spares could be operative, adding N phase centers for each spare. The link budget would also improve with the receiving antennas.

REFERENCES

[1] Tomiyasu, K., "Synthetic aperture radar in geosynchronous orbit," *Antennas and Propagation Society International Symposium, 1978*, vol. 16, pp.42-45, May 1978

[2] Madsen, S.N.; Chen, C.; Edelstein, W., "Radar options for global earthquake monitoring," *Geoscience and Remote Sensing Symposium, 2002. IGARSS '02*, vol.3, pp.1483-1485 vol.3, 2002

[3] Kou, L.; Xiang, M.; Wang, X.; Zhu, M., "Tropospheric effects on L-band geosynchronous circular SAR imaging," *Radar, Sonar & Navigation, IET*, vol.7, no.6, pp.693-701, July 2013

[4] Cheng, H.; Xiaorui, L.; Teng, L.; Yangte, G., "GEO SAR interferometry: Theory and feasibility study," *Radar Conference 2013, IET*, pp.1-5, 14-16 April 2013

[5] Qingjun, Z.; Yangte, G.; Wenjun, G.; Jiaoshan, L.; Ke, L., "3D orbit selection for regional observation GEO SAR", *Neurocomputing*, Vol. 151, no 2, pp.692-699, 2014

[6] Prati, C.; Rocca, F.; Giancola, D.; Guarnieri, A.M., "Passive geosynchronous SAR system reusing backscattered digital audio broadcasting signals," *Geoscience and Remote Sensing, IEEE Trans.* vol.36, no.6, pp.1973-1976, Nov 1998

[7] Ruiz-Rodon, J.; Broquetas, A.; Makhoul, E.; Monti Guarnieri, A.; Rocca, F., "Nearly Zero Inclination Geosynchronous SAR Mission Analysis With Long Integration Time for Earth Observation," *Geoscience and Remote Sensing, IEEE Trans.*, vol.52, no.10, pp.6379-6391, Oct. 2014

[8] Wadge, G.; Guarnieri, A.M.; Hobbs, S.E.; Schultz, D., "Potential atmospheric and terrestrial applications of a geosynchronous RADAR," *Geoscience and Remote Sensing Symposium (IGARSS)*, pp. 946-949, 13-18 July 2014

[9] Iannini, L.; Guarnieri, A.M., "Atmospheric Phase Screen in Ground-Based Radar: Statistics and Compensation," *Geoscience and Remote Sensing Letters, IEEE*, vol.8, no.3, pp.537,541, May 2011

[10] Bruno, D.; Hobbs, S.E., "Radar Imaging From Geosynchronous Orbit: Temporal Decorrelation Aspects," *Geoscience and Remote Sensing, IEEE Trans.*, vol.48, no.7, pp. 2924-2929, July 2010

[11] Recchia, A.; Monti Guarnieri, A.; Broquetas, A.; Ruiz-Rodon, J., "Assesment of atmospheric phase screen impact on Geosynchronous SAR," *Geoscience and Remote Sensing Symposium (IGARSS), 2014*, vol., no., pp.2253,2256, 13-18 July 2014

[12] Massonnet, D., "Capabilities and limitations of the interferometric cartwheel," *Geoscience and Remote Sensing, IEEE Trans.*, vol.39, no.3, pp.506-520, Mar 2001

[13] Krieger, G., "MIMO-SAR: Opportunities and Pitfalls," *Geoscience and Remote Sensing, IEEE Trans.*, vol.52, no.5, pp.2628,2645, May 2014

[14] Cristallini, D.; Pastina, D.; Lombardo, P., "Exploiting MIMO SAR Potentialities With Efficient Cross-Track Constellation Configurations for Improved Range Resolution," *Geoscience and Remote Sensing, IEEE Transactions on* , vol.49, no.1, pp.38,52, Jan. 2011

[15] Cazzani, L.; Colesanti, C.; Leva, D.; Nesti, G.; Prati, C.; Rocca, F.; Tarchi, D., "A ground-based parasitic SAR experiment," *Geoscience and Remote Sensing, IEEE Trans.*, vol.38, no.5, pp.2132-2141, Sep 2000

[16] Tebaldini, S.; Rocca, F.; Monti Guarnieri, A., "Model Based SAR Tomography of Forested Areas," *Geoscience and Remote Sensing Symposium, IGARSS 2008*, vol.2, no. II, pp. 593-596, 7-11 July 2008

[17] P. Wauthier, P. Francken and H. Laroche, "Co.location of six ASTRA satellites: assessment after one year of operations", *Space Flight Dynamics, 12th International Symposium,* ESOC, SP-403, Aug. 1997

[18] Moccia, A.; Renga, A., "Synthetic Aperture Radar for Earth Observation from a Lunar Base: Performance and Potential Applications," *Aerospace and Electronic Systems, IEEE Trans.*, vol.46, no.3, pp.1034-1051, July 2010

[19] Fornaro, G.; Franceschetti, G.; Lombardini, F.; Mori, A.; Calamia, M., "Potentials and Limitations of Moon-Borne SAR Imaging," *Geoscience and Remote Sensing, IEEE Trans.*, vol.48, no.7, pp.3009-3019, Jul 2010